Acknowledgments

The authors would like to thank the Kyoto University-Venture Business Laboratory for the use of their experimental laboratory. This study was supported by Agri-Health Translational Research Project (Ministry of Agriculture, Forestry and Fisheries of Japan).

Appendix A. Supplementary data

Supplementary data associated with this article can be found, in the online version, at doi:10.1016/j.bbrc.2012.02.130.

References

[1] A.M. Collinsworth, S. Zhang, W.E. Kraus, G.A. Truskey, Apparent elastic modulus and hysteresis of skeletal muscle cells throughout differentiation, Am. J. Physiol. Cell Physiol. 283 (2002) C1219–C1227.
[2] E.M. Darling, M. Topel, S. Zauscher, P.V. Thomas, F. Guilak, Viscoelastic properties of human mesenchymally-derived stem cells and primary osteoblasts, chondrocytes, and adipocytes, J. Biomech. 41 (2008) 454–464.
[3] E.M. Darling, P.E. Pritchett, B.A. Evans, R. Superfine, S. Zauscher, F. Guilak, Mechanical properties and gene expression of chondrocytes on micropatterned substrates following dedifferentiation in monolayer, Cell. Mol. Bioeng. 2 (2009) 395–404.
[4] H. Yu, C.Y. Tay, W.S. Leong, S.C.W. Tan, K. Lio, L.P. Tan LP, Mechanical behavior of human mesenchymal stem cells during adipogenic and osteogenic differentiation, Biochem. Biophys. Res. Commun. 393 (2010) 150–155.
[5] E. Schuh, J. Kramer, J. Rohwedel, H. Notbohm, R. Müller, T. Gutsmann, N. Rotter, Effect of matrix elasticity on the maintenance of the chondrogenic phenotype, Tissue Eng. Part A 16 (2010) 1281–1290.
[6] K. von der Mark, V. Gauss, H. von der Mark, P. Müller, Relationship between cell shape and type of collagen synthesised as chondrocytes lose their cartilage phenotype in culture, Nature 267 (1977) 531–532.
[7] P.D. Benya, J.D. Shaffer, Dedifferentiated chondrocytes reexpress the differentiated collagen phenotype when cultured in agarose gels, Cell 30 (1982) 215–224.
[8] K.R. Brodkin, A.J. García, M.E. Levenston, Chondrocyte phenotypes on different extracellular matrix monolayers, Biomaterials 25 (2004) 5929–5938.
[9] A. Yamamoto, S. Mishima, N. Maruyama, M. Sumita, Quantitative evaluation of cell attachment to glass, polystyrene, and fibronectin- or collagen-coated polystyrene by measurement of cell adhesive shear force and cell detachment energy, J. Biomed. Mater. Res. 50 (2000) 114–124.
[10] G. Hoben, W. Huang, B.S. Thoma, R.G. LeBaron, K.A. Athanasiou, Quantification of varying adhesion levels in chondrocytes using the cytodetacher, Ann. Biomed. Eng. 30 (2002) 703–712.
[11] W. Huang, B. Anvari, J.H. Torres, R.G. LeBaron, K.A. Athanasiou, Temporal effects of cell adhesion on mechanical characteristics of the single chondrocyte, J. Orthop. Res. 21 (2003) 88–95.
[12] C.C. Wu, H.W. Su, C.C. Lee, M.J. Tang, F.C. Su, Quantitative measurement of changes in adhesion force involving focal adhesion kinase during cell attachment, spread, and migration, Biochem. Biophys. Res. Commun. 329 (2005) 256–265.
[13] K. Yamamoto, N. Tomita, Y. Fukuda, S. Suzuki, N. Igarashi, T. Suguro, Y. Tamada, Time-dependent changes in adhesive force between chondrocytes and silk fibroin substrate, Biomaterials 28 (2007) 1838–1846.
[14] N. Cai, C.C. Wong, S.C.W. Tan, V. Chan, K. Liao, Temporal effect of functional blocking of β_1 integrin on cell adhesion strength under serum depletion, Langmuir 25 (2009) 10939–10947.
[15] Y. Kambe, K. Yamamoto, K. Kojima, Y. Tamada, N. Tomita, Effects of RGDS sequence genetically interfused in the silk fibroin light chain protein on chondrocyte adhesion and cartilage synthesis, Biomaterials 31 (2010) 7503–7511.
[16] Y. Kambe, Y. Takeda, K. Yamamoto, K. Kojima, Y. Tamada, N. Tomita N, Effect of RGDS-expressing fibroin dose on initial adhesive force of a single chondrocyte, Biomed. Mater. Eng. 20 (2010) 309–316.
[17] T. Atsumi, Y. Ikawa, Y. Miwa, K. Kimata, A chondrogenic cell line derived from a differentiating culture of AT805 teratocarcinoma cells, Cell Differ. Dev. 30 (1990) 109–116.
[18] C. Shukunami, C. Shigeno, T. Atsumi, K. Ishizeki, F. Suzuki, Y. Hiraki, Chondrogenic differentiation of clonal mouse embryonic cell line ATDC5 in vitro: differentiation-dependent gene expression of parathyroid hormone (PTH)/PTH-related peptide receptor, J. Cell Biol. 133 (1996) 457–468.
[19] N. Otsu, A threshold selection method from gray-level histograms, IEEE Trans. Syst. Man Cybern. B: Cybern. 9 (1979) 62–66.
[20] P. Castagnola, B. Dozin, G. Moro, R. Cancedda, Changes in the expression of collagen genes show two stages in chondrocyte differentiation in vitro, J. Cell Biol. 106 (1988) 461–467.
[21] L.C. Gerstenfeld, W.J. Landis, Gene expression and extracellular matrix ultrastructure of a mineralizing chondrocyte cell culture system, J. Cell Biol. 104 (1991) 1435–1441.
[22] K. Nagayama, Y. Nagano, M. Sato, T. Matsumoto, Effect of actin filament distribution on tensile properties of smooth muscle cells obtained from rat thoracic aortas, J. Biomech. 39 (2006) 293–301.
[23] S.C.W. Tan, W.X. Pan, G. Ma, N. Cai, K.W. Leong, K. Liao, Viscoelastic behaviour of human mesenchymal stem cells, BMC Cell Biol. 9 (2008) 40.
[24] M. Hirose, T. Ishizaki, N. Watanabe, M. Uehata, O. Kranenburg, W.H. Moolenaar, F. Matsumura, M. Maekawa, H. Bito, S. Narumiya, Molecular dissection of the Rho-associated protein kinase (p160ROCK)-regulated neurite remodeling in neuroblastoma N1E-115 cells, J. Cell Biol. 141 (1998) 1625–1636.
[25] M. Maekawa, T. Ishizaki, S. Boku, N. Watanabe, A. Fujita, A. Iwamatsu, T. Obinata, K. Ohashi, K. Mizuno, S. Narumiya, Signaling from Rho to the actin cytoskeleton through protein kinases ROCK and LIM-kinase, Science 285 (1999) 895–898.
[26] A. Woods, G. Wang, F. Beier, RhoA/ROCK signaling regulates Sox9 expression and actin organization during chondrogenesis, J. Biol. Chem. 280 (2005) 11626–11634.
[27] D. Kumar, A.B. Lassar, The transcriptional activity of Sox9 in chondrocytes is regulated by RhoA signaling and actin polymerization, Mol. Cell. Biol. 29 (2009) 4262–4273.
[28] B. Newman, L.I. Gigout, L. Sudre, M.E. Grant, G.A. Wallis, Coordinated expression of matrix Gla protein is required during endochondral ossification for chondrocyte survival, J. Cell Biol. 154 (2001) 659–666.
[29] T.D. Challa, Y. Rais, E.M. Ornan, Effect of adiponectin on ATDC5 proliferation, differentiation and signal pathways, Mol. Cell. Endocrinol. 323 (2010) 282–291.

TISSUE ENGINEERING: Part C
Volume 19, Number 5, 2013

DOI: 10.1089/ten.tec.2012.0424

Observation and Quantification of Chondrocyte Aggregation Behavior on Fibroin Surfaces Using Voronoi Partition

Akihisa Otaka, MEng,[1] Naoyoshi D. Kachi, PhD,[1] Naoya Hatano, BE,[1] Yoshihiko Kuwana, PhD,[2] Yasushi Tamada, PhD,[2] and Naohide Tomita, MD, PhD[1]

Cell migration is one of the fundamental processes in histogenesis, and it is necessary to investigate such multicellular behavior quantitatively in cell regeneration studies. In this study, Voronoi diagram analysis was first confirmed in simulation testing, and then used to evaluate the multicellular behavior of chondrocytes on three different substrates: (1) wild-type fibroin (FIB); (2) L-RGDSx2 transgenic fibroin; (3) and collagen. The indices for the round factor average, round factor homogeneity, and area disorder (AD), calculated from Voronoi diagram analysis, were used to characterize the difference in spatiotemporal changes for the different chondrocyte populations, and a regression analysis of the AD index was used to measure the speed of cell aggregation. The results suggested that the arginine-glycine-aspartic acid-serine sequence affects aggregate formation of chondrocytes cultured on FIB. The Voronoi diagram analysis represents one of the promising quantitative analyses for cell regeneration studies.

Introduction

LIVE-CELL OBSERVATION has become a powerful analytical tool in many cell biology laboratories because of advancements in microscopy techniques and cell imaging technologies.[1] On the other hand, evaluation methods for quantifying multicellular morphodynamics are still not yet fully developed. However, to successfully engineer artificial tissue constructs, some quantification tools for analyzing multicellular formation are necessary.[2]

For accurately evaluating the spatiotemporal formation of cell populations, there are two major requirements. First, automated visual tracking of the cells is necessary for quantitative and systematic analysis. Second, techniques that accurately characterize patterns of cell behavior, such as migration, proliferation, and apoptosis, are required. While visual tracking techniques have been studied extensively, less attention has been given to cell behavior characterization techniques.

In previous work, Kawakami *et al.* demonstrated that initial chondrocyte aggregation led to enhanced cartilage tissue formation in fibroin (FIB) sponges.[3] Additionally, cell aggregation is considered to be a key event in a wide range of fields, from tissue engineering to embryology and involves many types of cells, such as hepatocytes and chondrocytes,[3–5] as along with tumor and mesenchymal stem cells as well. This indicates that cell aggregation is one of the key events in cell-to-cell interaction, making it a vital part of tissue formation. However, in multicellular biophysics, evaluation of the cell aggregation process has been neither quantitative nor objective, but rather qualitative and highly researcher dependent. This lack of reliable and repeatable quantitative cell aggregation assays has made it difficult to investigate multicellular biophysics in the aggregate formation process.

The purpose of this study was to introduce the concept of "cellular sociology" into tissue engineering and bioenvironment design. This concept focuses on the social behavior of cell populations, which varies in response to the cells' surroundings and the physiological and phenotypical state of the cells themselves. Moreover, by understanding the relationship between cell population and extracellular environment, it is possible to gain insights into a wide range of cell biophysics (e.g., cell–cell and cell–substrate/material interactions). In the field of cellular sociology, cell arrangement analysis using a Voronoi diagram is one of the most successful methods for the evaluation of different cell populations. Voronoi analysis has been used previously to evaluate the spatiodistribution of retinal,[6] cortical,[7] and tumor cells.[8–11] Nawrocki Raby *et al.* evaluated the process of tumor cell cohesion using graphical quantification, including Voronoi diagram analysis, and concluded that this method represented a new way to predict the aggressiveness of various tumor cells.[9] In a similar fashion, Voronoi diagram analysis may provide new insights into the multicellular biophysics involved in tissue regeneration and allow for improved computational modeling of cell behavior in scaffolds.

[1]Department of Mechanical Engineering and Science, Kyoto University Graduate School of Engineering, Kyoto, Japan.
[2]National Institutes of Agrobiological Sciences, Tsukuba, Japan.

In this study, two types of experiments were performed. First, Marcelpoil and Usson's distribution assay,[12] which has been used in the study of tumor cell distribution,[9,11] was examined with respect to its validity as a method for evaluating chondrocyte aggregation on different substrates. Specifically, to confirm the relationship between cell aggregation and various analysis metrics, unambiguous examples of different aggregation patterns were simulated and analyzed in a set of *in silico* experiments. After confirming these relationships, a number of *in vitro* experiments were then performed to examine the spatiotemporal distributions of chondrocytes on three different substrates: (1) collagen (CON); (2) FIB; and (3) RGD-transgenic fibroin, which was created by genetically interfusing arginine-glycine-aspartic acid-serine (RGDS) peptides into silk FIB molecules.[13] It was reported previously that chondrocyte aggregation is enhanced in FIB sponges,[3] but chondrocyte aggregation behavior on FIB has yet to be evaluated quantitatively. Thus, the objective of this study was to quantitatively assess whether FIB enhances cell aggregation behavior using *in silico* validated Voronoi diagram analysis methods.

Materials and Methods

Cell population quantification

The spatial distribution of cells was characterized and quantified using a cellular sociology algorithm based on geometrical models, as described by Marcelpoil and Usson[12] (i.e., Voronoi's partition). These methods, applied to the set of points that relate to the position of the cells (Fig. 1), provide information about the spatial distribution and neighborhood relationships of the cells. From the Voronoi diagram, three quantitative parameters can be deduced: (1) average and standard deviation of the areas (round factor average [RFav]); (2) roundness factor homogeneity (RFH); and (3) area disorder (AD). Each index was calculated using the equations derived by Marcelpoil and Usson.[12] As is customary, border zones of the Voronoi diagram were excluded from the analysis, as no information can be taken relating to the final position of cells in these zones.

In silico *experiment: simulation of aggregate cell populations*

Model formulation. Cell aggregations can vary in their size, cell density, and gathering potential. A computer simulation model was conducted to examine whether cell population affects the RFav, RFH, and AD indexes during aggregation. Three cell population models (type A, type B, and type C; described in section "Model of cell arrangement") that were observed regularly in our time-lapse observation were simulated. Afterward, the cell distribution points were evaluated using a Voronoi diagram. Every trial was executed and evaluated six times.

Model of cell arrangement. Three types of cell distribution were created using 100 separate points set on a 2D plane using the procedures described below. (Note: Cells were not placed at the exact nodal points of the square lattice, but rather randomly scattered around each node using a Gaussian distribution with a standard deviation of 10 pixels (Fig. 2).

Type A: This model was used to analyze the effect of cell density. Using a 10×10 array of points located at the nodes of a perfect square lattice, groups with high, medium, and low cell density were simulated by changing the mesh size of the square lattice to 30 (high density; H), 60 (middle density; M), and 90 pixels (low density; L), respectively. A control group (C) in which the population was distributed randomly (Fig. 3, model A) was also created.

Type B: This model was used to evaluate the rate at which cells participated in aggregation. Using an array of N points located at the nodes of a square lattice and 100-N points distributed randomly, groups with 0%, 25%, 50%, 75%, and 100% aggregation participation ratios were simulated by changing the N value to 0, 25, 50, 75, and 100, respectively (Fig. 3, model B).

Type C: This model was used to analyze the effect of aggregate size. Using point forming groups, three types of cell populations were created in which cells formed: one large aggregate (AGG:1); two smaller aggregates (AGG:2); and four aggregates (AGG:4) that were smaller still. Each nodule

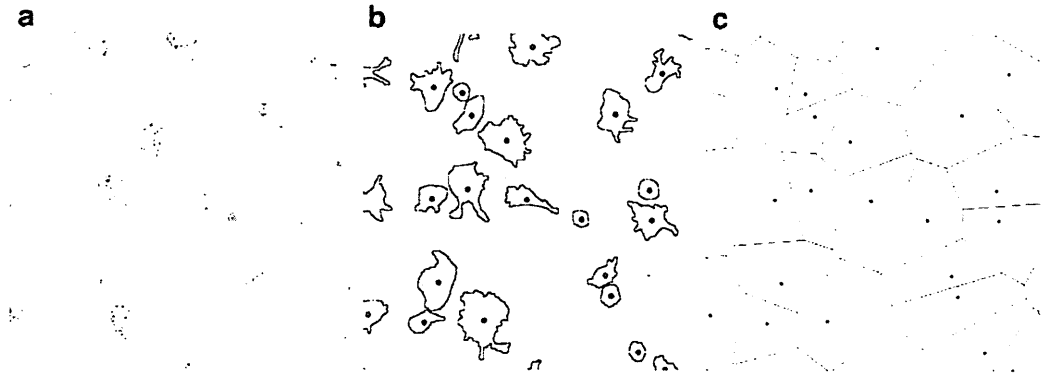

FIG. 1. Representation of the data acquisition process. **(a)** Example of typical cartilage observation on a polydimethylsiloxane surface with a phase-contrast microscope. **(b)** Outlines and center points of cells extracted from snapshot images. **(c)** The derived Voronoi polygon using the point set of cell centers created by the Open Computer Vision Library (http://opencv.willowgarage.com/wiki/). Scale bar=20 μm.

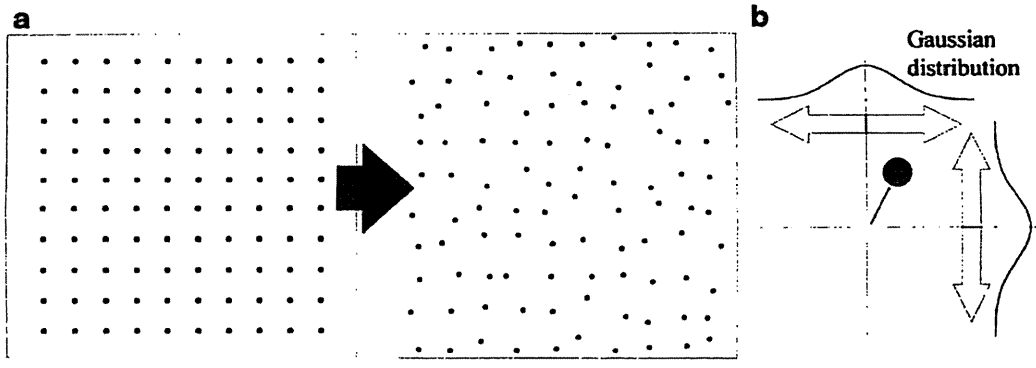

FIG. 2. Schematic model of an aggregating cell population. (a) Randomization of the point set ordered at the nodes of a square lattice. (b) Spatial perturbation of a point in XY coordinates according to the Gaussian distribution with a standard deviation of 10 pixels.

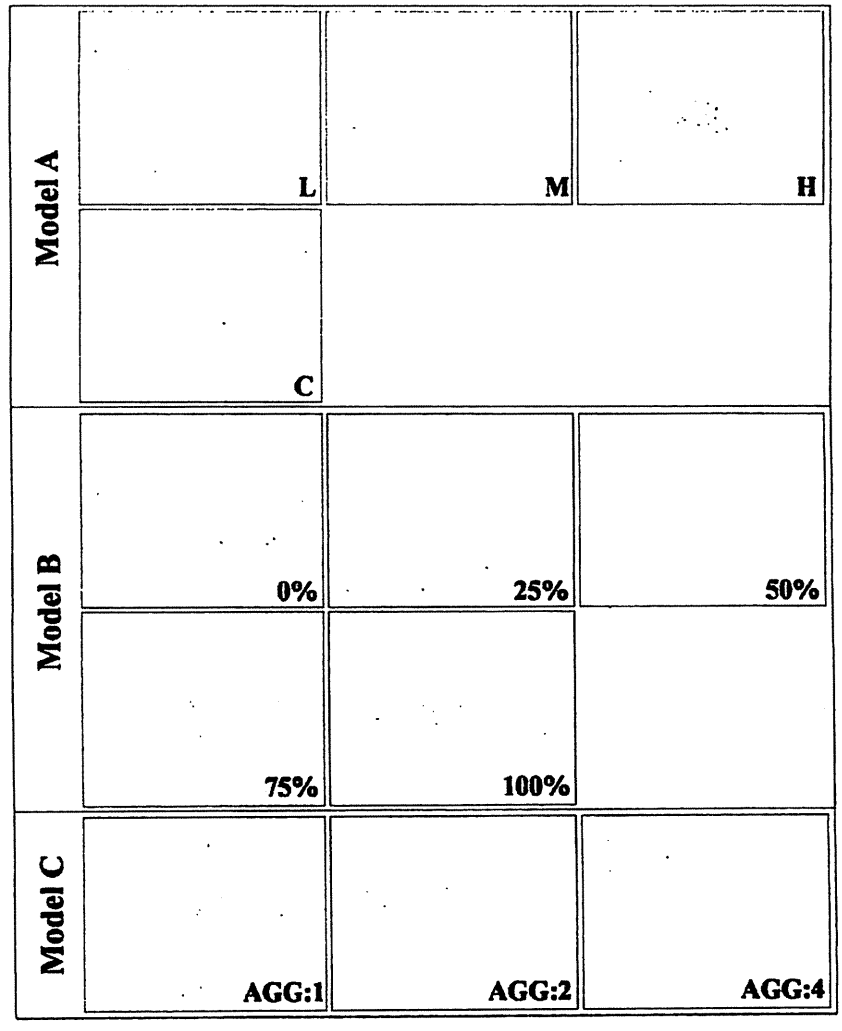

FIG. 3. Representative image of aggregation models. Each model was varied in the degree of cell density (type A), cell aggregation participation ratio (type B), and the number of cells within each aggregrate (type C).

had the same size and contained 100, 50, and 25 points, respectively (Fig. 3, model C).

In vitro *experiment: cell seeding experiment in 2D culture*

Chondrocyte preparation. Articular cartilage tissue was aseptically removed from the proximal humerus, distal femur, and proximal tibia of 4-week-old Japanese White rabbits (Oriental Bio Service Co., Ltd.). After any adherent connective tissue had been removed, the excised cartilage tissue was diced into 1-mm^3 segments and chondrocytes were isolated by digesting small segments of cartilage with 0.25% trypsin-ethylenediaminetetraacetic acid (EDTA) (Nacalai Tesque, Inc.) for 30 min in a temperature-controlled bath at 37°C. After being rinsed twice with Dulbecco's phosphate-buffered saline (PBS; Nacalai Tesque, Inc.) and centrifuged at 1500 rpm for 5 min, the cartilage was enzymatically digested with 0.25% type II collagenase (CLS-2; Worthington Biochemical Co.) for 6 h at 37°C. After staining through a cell strainer (BD Falcon, Inc.) and washing twice with PBS, a single-cell suspension was obtained. Cartilage harvests from living animals were approved and accepted by the animal care committee of the Institute for Frontier Medical Sciences at the Kyoto University.

Cells were passaged once in T-flasks (Iwaki Glass Co., Ltd.) with the Dulbecco's modified Eagle's medium (DMEM; Nacalai Tesque, Inc.) containing 10% fetal bovine serum (FBS; Nacalai Tesque, Inc.) and 1% antibiotic mixture (10,000 U/mL penicillin, 10,000 mg/mL streptomycin, and 25 mg/mL amphotericin B; Nacalai Tesque, Inc.) before experimentation. Cells were cultured at 37°C in a humidified atmosphere of 95% air and 5% CO_2 for 5 days, and the medium was changed every 2 days.

Substrate preparation. A polydimethylsiloxane (PDMS) liquid solution was prepared by using a SYLGARD 184 SILICONE ELASTOMER KIT (Dow Corning Toray Co., Ltd.) and curing for 48 h at room temperature in a culture dish (diameter, 150 mm; Asahi Glass Co., Ltd.). Afterward, the PDMS sheet was cut into disks that were 2 mm in thickness and 35 mm in diameter. Disks were sterilized by autoclave before experimentation.

CON, wild-type FIB, and L-RGDSx2 fibroin (LRF) were used as substrate coatings and prepared using the procedures listed below. Three substrate-coated disks were prepared for each substrate (CON, FIB, and LRF) and set in a culture dish (diameter, 35 mm; Asahi Glass Co., Ltd.). Each substrate disk was washed twice with PBS before use.

CON substrate: As a control, type I collagen-coated PDMS disks were used, with PDMS chosen due to its hydrophobic nature. The PDMS disks were soaked in 10% Cellmatrix Type I-C (Nitta gelatin, Inc.) diluted in HCl (pH 3.0, 1 mM) for 30 min at room temperature. Afterward, the plates were washed with a culture medium (DMEM) three times and with PBS twice thereafter.

FIB substrate: A FIB aqueous solution was prepared as described previously.[5,14] Briefly, degummed silk FIB fibers from *Bombyx mori* cocoons were dissolved in a 9 M lithium bromide aqueous solution at room temperature, with the solution subsequently dialyzed against pure water. The concentration of FIB in the water solution was determined by the colorimetric method and was prepared to be 1% (wt/vol). Before coating the FIB substrate, PDMS disks were treated with O_2 plasma to make the surface hydrophilic. The PDMS disks were then soaked in the FIB aqueous solution for 1 h at room temperature and dried at 50°C. The coated disks were immersed in an 80% methanol solution for 1 h and dried again at 50°C.

LRF substrate: The LRF is a protein in which (RGDS)x2 sequences have been fused with FIB L-chains at the amino-terminus. An LRF aqueous solution was prepared using the same technique as that used for the preparation of the wild-type FIB aqueous solution. PDMS disks coated with LRF were also manufactured in the same process as that used for the wild-type FIB samples.

Time-lapse microscopy. Passaged chondrocytes were removed from T-flasks by adding 0.25% trypsin-EDTA and washing twice with PBS. Shortly after detachment, cells were suspended in the Leibovitz's L-15 medium (Invitrogen Corp.) containing 10 vol% FBS, and 1 vol% antibiotic mixture and seeded on substrate dishes at a concentration of 1.5×10^4 cells/cm^2. Following that, the dish was placed on an inversion microscope (IX-71; Olympus Corp.) and enclosed in a small transparent culture chamber (MI-IBC-IF; Olympus Corp.) with in a humidified atmosphere at 37°C. A 10× magnification objective lens (CPlan N 10x/0.25 PhC; Olympus Corp.) was used in our experiment. During a 24-h culture, time-lapse phase-contrast images were captured every 10 min by a CCD camera (DP70; Olympus Corp.).

Chondrocyte distribution quantitation. To acquire positional datum related to the chondrocytes' distribution, the images, captured at 10 min, and 3, 6, 9, 12, and 24 h after seeding, were analyzed according to the following procedure. Each cell was outlined and painted over manually using Photoshop (Adobe Systems, Inc.) and cell binary images were generated. Afterward, the cell positions were sorted out using the Particles Analysis command in ImageJ (National Institutes of Health) (Fig. 1). Using this population data, Voronoi diagrams were produced and three indexes (AD, RFav, RFH) were calculated. The number of cells was also recorded, and the rate of cell growth was calculated by dividing the number of cells in each time step by the initial number of cells. Time-dependent changes in AD were fitted to a nonlinear regression model.

Statistical analysis and data presentation

Experimental values in each figure are presented as mean ± standard deviation. One-way analysis of variance (ANOVA) and a Tukey's test for *post hoc* comparison were done to analyze the significance of time-dependent changes in RFH, RFav, AD, and the rate of cell growth in *in vitro* experiments. A Student's *t*-test was done to analyze the significance between the groups in the *in vitro* experiment. All statistical tests were determined using a criterion of $p < 0.05$. An asymptotic exponential curve was used for regression analysis of the temporal AD changes on each substrate.

Results

The outcomes from in silico experiments

The RFav versus RFH versus AD shown in Figure 4 describes the results for RVav, RFH, and AD in the *in silico* experiments. These results were calculated from cell simulations

using type A (Fig. 4a), type B (Fig. 4b), and type C (Fig. 4c) cell populations. In these conditions, RFav, RFH, and AD ranged from 0.65 to 0.80, from 0.74 to 0.90, and from 0.31 to 0.72, respectively.

The statistical significance analysis indicates that RFav is insensitive to the rate at which cells participate in aggregation (Fig. 4b), and that RFH is insensitive to the number of cells involved in aggregation (Fig. 4c). On the other hand, AD results reveal a significant difference between multiple groups for all simulation types. Thus, AD appears to be more sensitive than RFav and RFH in evaluating aggregating cell populations, especially with respect to aggregate cell density and the ratio of cells involved in aggregation.

The outcomes from in vitro *experiments*

In Figure 5, chondrocytes on each substrate are shown after 12 and 24 h of culture time. On the CON substrate, chondrocytes elongated and few cells were found to be in contact with each other (CON). On both FIB substrates (FIB and LRF), most chondrocytes maintained a rounded shape and participated in cell aggregation. Chondrocytes on these substrates were active in migration during the early stages of cell culture, but cell speed appeared to decrease with cell aggregation. Compared with the LRF substrate, the aggregation size was larger and fewer cells remained solitary on the FIB substrate.

Chondrocytes on the FIB and LRF substrates did not increase significantly in the 24-h culture period, as shown in Figure 6. Only on the CON substrate was significant cell growth observed ($p<0.01$, one-way ANOVA). Furthermore, significant differences in the temporal cell growth on the CON substrate were found only between 10 min–24 h ($p<0.01$), 3–24 h ($p<0.01$), and 12–24 h ($p<0.05$, Tukey test) of culture time. Thus, there were no significant changes in cell proliferation during the first 12 h after seeding on each surface.

The time-dependent changes in RFav, RFH, and AD for chondrocytes grown on each substrate are shown in Figure 7. The initial value for each index was almost the same for each substrate, but the RFav and AD values for the FIB substrate and all three indices for the LRF substrate changed significantly over the 24-h culture period ($p<0.05$, one-way ANOVA). The absence of change in the indexes recorded for the

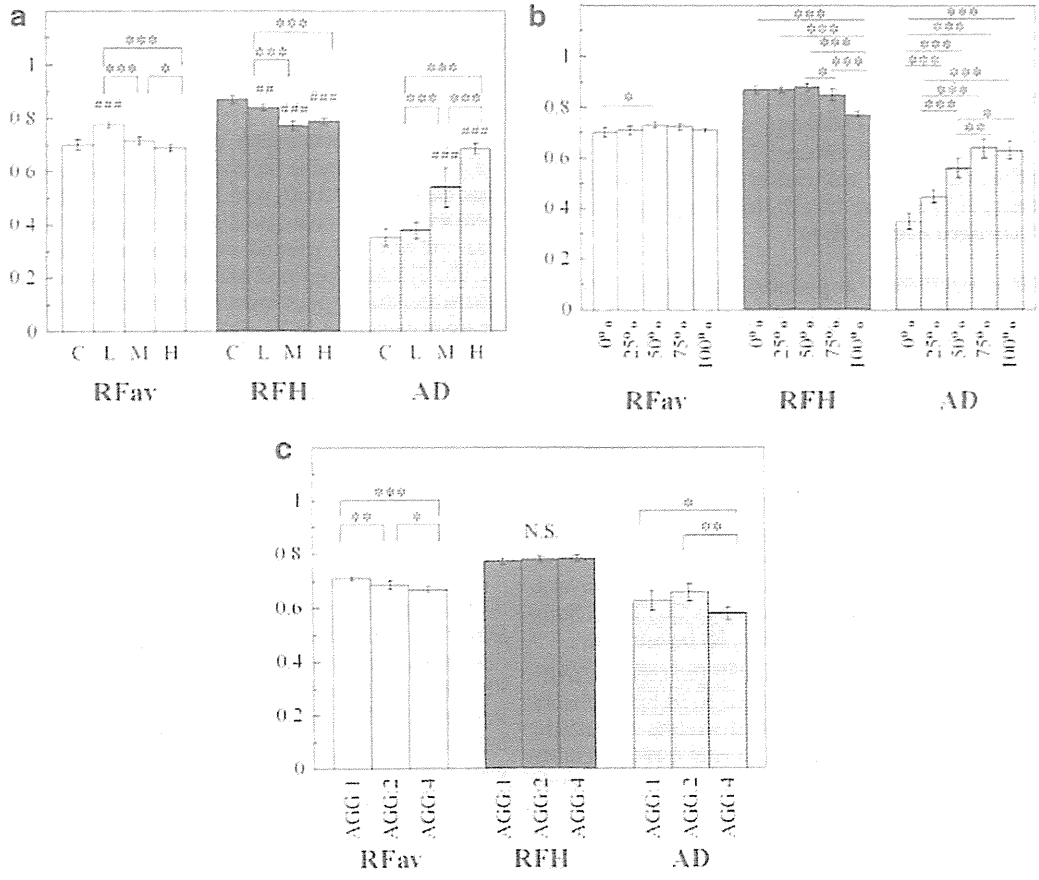

FIG. 4. Derived round factor average (RFav), roundness factor homogeneity (RFH), and area disorder (AD) from model type A [(a) differ in cell density], model type B [(b) differ in aggregate participation], and model type C [(c) differ in aggregate size]. In (a), $^{*,\#}p<0.05$, $^{\#\#}p<0.01$, $^{***,\#\#\#}p<0.001$; by Tukey–Kramer test. *Indicates significance between model groups, and #indicates significance between model groups and control groups. In (b) and (c), $^{*}p<0.05$, $^{**}p<0.01$, $^{***}p<0.001$; by Tukey–Kramer test. Error bars indicate square distributions; $n=6$.

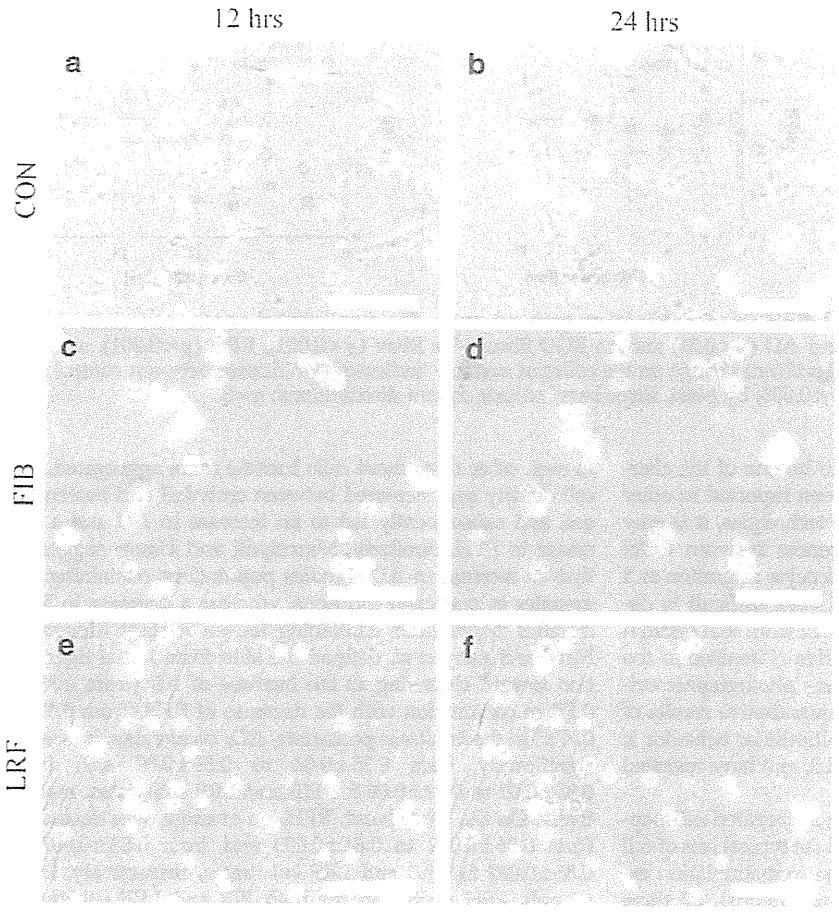

FIG. 5. Phase-contrast images of chondrocytes cultured on collagen (a, b), on wild-type fibroin (c, d), and on RGD fibroin surfaces (c, f), which were taken 12 h (a, c, e) and 24 h (b, d, f) after seeding. Scale bar = 20 μm.

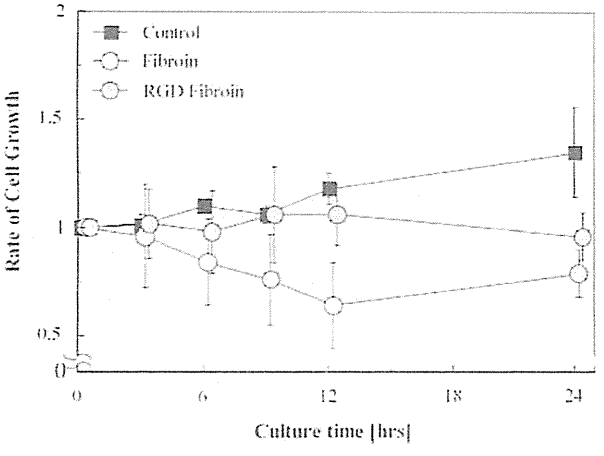

FIG. 6. Temporal changes in chondrocyte growth rate on each substrate. The significant change in the number of observed chondrocytes was seen only on the collagen surface by one-way analysis of variance. Error bars indicate square distributions; $n = 3$.

CON substrates was probably caused by the cells lack of aggregation. Asymptotic exponential curves were fitted to the mean values of the AD index in a time-dependent manner for every substrate (Fig. 8) The relaxation time was 1.56 for the FIB substrate and 4.39 for the LRF substrate, and the AD values for the FIB and LRF substrates were fixed at 0.54 and 0.49, respectively, during the 24-h culture period.

Discussion

The purpose of this study was to investigate how best to quantitatively characterize cell populations in various culture conditions. The results of simulation testing showed that RFav and RFH were insensitive to the rate at which cells participated in aggregation and the number of cells involved in aggregation, respectively. However, there appeared to be a direct relationship between AD and the degree of aggregation, with increasing AD values observed for increasing cell aggregation. The significance of this relationship was confirmed statistically (Tukey–Kramer test, $p < 0.05$). Using this information, the results of the *in vitro* experiments were analyzed and the cell aggregation behavior on the different substrates analyzed. According to the time-dependent changes in AD, the FIB surface seems to be quite different from the CON surface with respect to multicellular behavior.

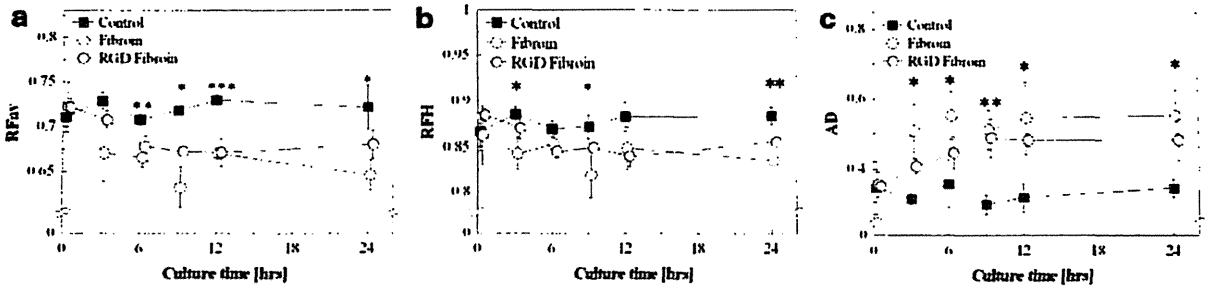

FIG. 7. Temporal changes in RFav (a), RFH (b), and AD (c) on each substrate. The significant changes were observed on wild-type fibroin for RFav ($p<0.01$) and AD ($p<0.01$) and on RGD fibroin for RFav ($p<0.001$), RFH ($p<0.001$), and AD (0.05). All three indexes exhibited no significant change on the collagen surface. *indicates significance between control and fibroin groups. *$p<0.05$, **$p<0.01$, ***$p<0.005$; by t-test. Error bars indicate square distributions; $n=3$.

Promotion of cell aggregation seems to be one of the characteristics of FIB substrates, and has been reported in other studies as well.[3,5] Using observational techniques, it is easy to qualitatively distinguish the differences between CON and FIB surfaces with respect to chondrocyte migration and population (Fig. 5a, b). However, it is quite difficult to determine whether wild-type FIB is different from RGD fibroin in terms of cell population, because this difference is too subtle to discern simply from observing photographic evidence (Fig. 5b, c). In that respect, the quantitative results of this study have demonstrated that multicellular behavior is affected by the coating substrate material, and have revealed different time-dependent processes.

There are few criteria for evaluating aggregated cell populations using a Voronoi diagram; so, three typical sets of cell population distribution were conducted in a simulation experiment. In the aggregation distribution model, all three indexes (AD, RFav, and RFH) changed according to the degree of cell density (type A), the degree of cell participation in aggregating (type B), and the number of cells in a single aggregate (type C). In types A and B, as the cells came closer to each other or as more cells became more aggregated, the cell density gap increased between crowded and barren areas, and subsequently led to an increase in AD and a decrease in RFH. Similarly, Marcelpoil and Usson suggested that an increase in AD signifies populations containing aggregates in particular locations, whereas a decrease in RFH signifies populations containing barren islets.[12] Moreover, Nawrocki Raby *et al.* defined the shift from initial distribution toward clustering as the increase of AD (from 0.33 to 0.57) in conjunction with the decrease of RFH (from 0.80 to 0.77).[9] In the *in vitro* experiments, AD, on average, increased significantly from 0.35 ± 0.04 to 0.55 ± 0.07 and from 0.35 ± 0.02 to 0.48 ± 0.06 for FIB and LRF substrates, respectively. On the other hand, RFH, on average, was decreased from 0.86 ± 0.032 to 0.84 ± 0.003 and from 0.88 ± 0.007 to 0.86 ± 0.002 for FIB and LRF substrates, respectively. Even though, RFH decreased for both FIB and LRF substrates, statistical significances were detected only for LRF.

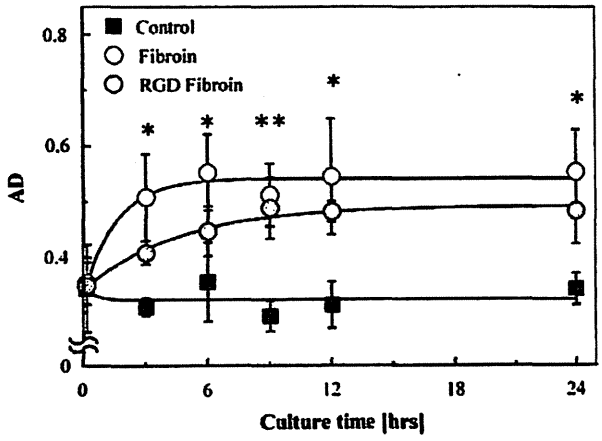

FIG. 8. Regression analysis of temporal AD changes for each substrate, resulting in a fit with R^2 of 0.13 (collagen), 0.96 (wild-type fibroin), and 0.99 (RGD fibroin). Each AD value converged to 0.32, 0.54, and 0.49, with a relaxation time of 0.44, 1.56, and 4.39 h, on collagen, wild-type fibroin, and RGD fibroin, respectively. *indicates significance between control and fibroin groups. *$p<0.05$, **$p<0.01$; by t-test.

There is one considerable reason why RFH did not change significantly. When less than half of the cells are in aggregation in simulation model type B, RFH values remain around 0.76, whereas RFH sensitively decreases when more than half of the cells are aggregated. In addition, it seems that cell density in a cluster can also affect RFH values. Based on the results above, the RFH index varies only in the latest phase of aggregation process when a majority of cells come close to each other. On the other hand, the AD index increases gradually with cell aggregation in model types A and B. So, as far as evaluating chondrocyte aggregation on FIB surfaces (like in Fig. 5), AD is more appropriate than RFH. In fact, temporal changes in AD matched well with the qualitative impressions observed experimentally.

The degree of aggregate formation has been expressed subjectively in the histomorphology field. The AD index seems to best characterize cell-aggregate populations among the three indexes of the Voronoi Diagram under the hypotheses that positive correlation with models A (H, M, and L) and B (0%, 25%, 50%, 75%, and 100%) together with no correlation with model C (AGG1, AGG2, and AGG3) agrees with the subjective criteria for aggregation. From time-lapse microscopy, most events in cell aggregation were observed during the first 12 h after seeding, with cell migration subsequently normalizing, followed by cell–cell adhesion. From this analysis, chondrocyte aggregation was supposed to be a relaxation process; hence, regression analysis was performed

to fit the temporal AD changes recorded for each substrate into an asymptotic exponential model. As a result, the decrease in relaxation time between FIB and LRF suggests that regression analysis of AD can be used to assess whether culture substrates can affect the cell aggregation process. Interestingly, the aggregation speed was delayed from 1.56 to 4.39 h on the RGDSx2 peptide interfused FIB substrate.

An RGD amino acid sequence is the minimum unit of a cell–substrate adhesive activity domain, which is a ligand of integrin.[15,16] Ryan *et al.* reported that decreasing substratum adhesiveness might lead to a slower rate of cell aggregation spreading over the substrate.[17] Moreover, Briggs *et al.* reported that the weakening of cell–substrate adhesion and the formation of cell aggregates were observed simultaneously and also accompanied the osteogenic differentiation of mesenchymal stem cells.[18] These results suggest that a balance between cell–cell and cell–substrate adhesion is one of the important factors in predicting cell aggregate formation/deformation. On the other hand, Kambe *et al.* reported that RGDSx2 peptide interfused into silk FIB significantly increased the cell adhesive force until 12 h after seeding.[19] Taking the above into consideration, it may be possible that cell–substrate adhesiveness decreases the tendency and speed of chondrocyte aggregate formation as the adhesive force of FIB increases.

AD analysis may be able to evaluate the motility of cellular aggregates, especially with respect to speed, which is not measured in qualitative observation. However, there are many hurdles that still remain to be cleared before this method is ready for use in tissue engineering. One of the most important problems that need to be addressed is how to translate multicellular behavior indices into design criteria for biological tissue growth. Certainly, the mechanisms underlying regeneration processes are regulated by not only by cytoskeletal-mediated force transmission factors, such as integrin and cadherin, but also by a network of genetic or biochemical signaling pathways. For the FIB scaffold design, it is still unclear how the chondrocyte aggregation process affects the maintenance of the cartilaginous phenotype during tissue regeneration; hence, genetical or histological surveys are needed in future studies. Moreover, cell aggregation must be assessed carefully, because cell motility and cohesion are phenomena that are central to cell organization within tissue scaffolds. Lauffenburger *et al.* stated that maximally useful engineering design principles for cell organization within tissue structures will require the most comprehensive models for cell motility behavior to be able to predict multicellular organization from quantifiable characteristics of cell–matrix and cell–cell interactions.[20] In this respect, AD is an unrefined, but easy-to-use tool for characterizing cell aggregation, and can be one of the approaches used to investigate spatiotemporal characteristics of cell–matrix and cell–cell interactions.

Conclusions

The findings obtained from this study are the following: (1) Three indexes (RFav, RFH, and AD) of the Voronoi diagram identified the differences in spatiotemporal changes between chondrocytes grown on FIB and CON surfaces; (2) The regression analysis of the AD index revealed the speed of cells during aggregation; and (3) Transgenic RGDS sequences reduced the aggregate formation of chondrocytes cultured on FIB.

Acknowledgments

We would like to thank Alex Turner for helping to improve the manuscript; the Kyoto University Venture Business Laboratory and the Institute for Frontier Medical Sciences of Kyoto University for use of their facilities. This work was supported by the Grant-in-Aid for the Creative Scientific Research from the Japan Science and Technology Agency; the Agri-Health Translational Project from the Ministry of Agriculture, Forestry and Fisheries, Japan; and the Student venture support system grant from the Advanced Scientific Technology and Management Research Institute of Kyoto.

Disclosure Statement

No competing financial interests exist.

References

1. Terryn, C., Bonnomet, A., Cutrona, J., Coraux, C., Tournier, J.-M., Nawrocki-Raby, B., *et al.* Video-microscopic imaging of cell spatio-temporal dispersion and migration. Crit Rev Oncol Hematol **69**, 144, 2009.
2. Liu, W.F., and Chen, C.S. Cellular and multicellular form and function. Adv Drug Deliv Rev **59**, 1319, 2007.
3. Kawakami, M., Tomita, N., Shimada, Y., Yamamoto, K., Tamada, Y., Kachi, N., *et al.* Chondrocyte distribution and cartilage regeneration in silk fibroin sponge. Biomed Mater Eng **21**, 53, 2011.
4. Kim, M.-H., Kino-oka, M., Morinaga, Y., Sawada, Y., Kawase, M., Yagi, K., *et al.* Morphological regulation and aggregate formation of rabbit chondrocytes on dendrimer-immobilized surfaces with D-glucose display. J Biosci Bioeng **107**, 196, 2009.
5. Kachi, N.D., Otaka, A., Sim, S., Kuwana, Y., Tamada, Y., Sunaga, J., *et al.* Observation of chondrocyte aggregate formation and internal structure on micropatterned fibroin-coated surface. Biomed Mater Eng **20**, 55, 2010.
6. Martinez Mozos, O., Bolea, J.A., Ferrandez, J.M., Ahnelt, P.K., and Fernandez, E. V-Proportion: a method based on the Voronoi diagram to study spatial relations in neuronal mosaics of the retina. Neurocomputing **74**, 418, 2010.
7. Minciacchi, D., Kassa, R.M., Del Tongo, C., Mariotti, R., and Bentivoglio, M. Voronoi-based spatial analysis reveals selective interneuron changes in the cortex of FALS mice. Exp Neurol **215**, 77, 2009.
8. Bigras, G., Marcelpoil, R., Brambilla, E., and Brugal, G. Cellular sociology applied to neuroendocrine tumors of the lung: quantitative model of neoplastic architecture. Cytometry **24**, 74, 1996.
9. Nawrocki Raby, B., Polette, M., Gilles, C., Clavel, C., Strumane, K., Matos, M., *et al.* Quantitative cell dispersion analysis: new test to measure tumor cell aggressiveness. Int J Cancer **93**, 644, 2001.
10. Zahm, J.M., Hazgui. S., Matos, M., Ben Seddik, A., Nawrocki Raby, B., Polette, M., *et al.* Quantitative videomicroscopic analysis of the sociologic behavior of non-invasive and invasive tumor cell lines. Cell Mol Biol **52**, 54, 2006.
11. Matos, M., Nawrocki Raby, B., Zahm, J.-M., Polette, M., Birembaut, P., and Bonnet, N. Cell migration and proliferation are not discriminatory factors in the *in vitro* sociologic

behavior of bronchial epithelial cell lines. Cell Motil Cytoskeleton **53**, 53, 2002.
12. Marcelpoil, R., and Usson, Y. Methods for the study of cellular sociology: Voronoi diagrams and parametrization of the spatial relationships. J Theor Biol **154**, 359, 1992.
13. Tamura, T., Thibert, C., Royer, C., Kanda, T., Abraham, E., Kamba, M., *et al.* Germline transformation of the silkworm *Bombyx mori* L. using a piggyBac transposon-derived vector. Nat Biotechnol **18**, 81, 2000.
14. Aoki, H., Tomita, N., Morita, Y., Hattori, K., Harada, Y., Sonobe, M., Wakitani, S., and Tamada, Y. Culture of chondrocytes in fibroin-hydrogel sponge. Biomed Mater Eng **13**, 309, 2003.
15. Ruoslahti, E., and Pierschbacher, M.D. Arg-Gly-Asp: a versatile cell recognition signal. Cell **44**, 517, 1986.
16. Ruoslahti, E., and Pierschbacher, M.D. New perspectives in cell adhesion: RGD and integrins. Science **238**, 491, 1987.
17. Ryan, P., Foty, R., Kohn, J., Steinberg, M.S.. Tissue spreading on implantable substrates is a competitive outcome of cell-cell vs. cell-substratum adhesivity. Proc Natl Acad Sci U S A **98**, 4323, 2001.
18. Briggs, T., Treiser, M.D., Holmes, P.F., Kohn, J., Moghe, P.V., and Arinzeh, T.L. Osteogenic differentiation of human mesenchymal stem cells on poly (ethylene glycol)-variant biomaterials. J Biomed Mater Res A **91**, 975, 2009.
19. Kambe, Y., Yamamoto, K., Kojima, K., Tamada, Y., and Tomita, N. Effects of RGDS sequence genetically interfused in the silk fibroin light chain protein on chondrocyte adhesion and cartilage synthesis. Biomaterials **31**, 7503, 2010.
20. Lauffenburger, D.A., and Griffith, L.G. Who's got pull around here? Cell organization in development and tissue engineering. Proc Natl Acad Sci U S A **98**, 4282, 2001.

Address correspondence to:
Naohide Tomita, MD, PhD
C3b s01 Graduate School of Engineering
Kyoto University
Kyoto daigaku-Katsura
Nishikyo-ku
Kyoto 615-8540
Japan

E-mail: tomita.naohide.5c@kyoto-u.ac.jp

Received: July 12, 2012
Accepted: October 16, 2012
Online Publication Date: January 31, 2013

///VSP///

Journal of Biomaterials Science 24 (2013) 158–169

Journal of BIOMATERIALS SCIENCE
brill.nl/jbs

Quantitative Evaluation of Fibroblast Migration on a Silk Fibroin Surface and TGFBI Gene Expression

Tomoko Hashimoto [a], Katsura Kojima [a], Akihisa Otaka [b], Yuji S. Takeda [b], Naohide Tomita [b] and Yasushi Tamada [a,*]

[a] Silk Materials Research Unit, Genetically Modified Organism Research Center, National Institute of Agrobiological Sciences, 1-2 Owashi, Tsukuba, Ibaraki 305-8634, Japan

[b] Department of Mechanical Engineering, Graduate School of Engineering, Kyoto University, Yoshida-Honmachi, Sakyo-ku, Kyoto 606-8501, Japan

Received 14 November 2011; accepted 27 January 2012

Abstract

Cell migration plays important roles in natural processes involving embryonic development, inflammation, wound healing, cancer metastasis and angiogenesis. Cell migration on various biomaterials is also believed to improve the rate of wound healing and implant therapies in the tissue-engineering field. This study measured the distance traversed, or mileage, of mouse fibroblasts on a silk fibroin surface. Fibroblasts on the fibroin surface moved with better progress during 24 h than cells on collagen or fibronectin surfaces. Results obtained by quantitative real-time reverse transcription-polymerase chain reaction (qRT-PCR) revealed that fibroblasts on the fibroin surface expressed transforming growth factor β-induced protein (TGFBI), which is an extracellular matrix (ECM) protein, stronger than on other surfaces in the early cell-culture stages. These results demonstrate that the fibroin surface shows higher potential to enhance cell migration and the production of ECM than a collagen or fibronectin surface.

Keywords

Silk fibroin, cell migration, fibroblast, ECM

1. Introduction

Silk, which is produced by silkworms (*Bombyx mori*), has been used commercially as a textile fiber because of its excellent properties for use in clothing: good mechanical strength, softness, luster and smooth texture. Furthermore, silk fiber has a long history of use as surgical suture. Its safety performance, such as long-term non-carcinogenicity and acute and chronic inflammatory reactions,

* To whom correspondence should be addressed. Tel./Fax: (81-29) 838-6164; e-mail: ytamada@affrc.go.jp

DOI:10.1163/156856212X629025

has been well studied [1]. Silk fibroin, a naturally derived polymer, is the main component of silk fiber. Silk fibroin can be fabricated into films, gels, sponges, resins and nanofibers using water solvent processes [2–8]. Many reports have described silk fibroin application to produce artificial veins and wound dressings, and have explained its applications in biomedical fields as a substrate for immobilized enzymes, as an anticoagulant material, an anti-HIV material, a substrate for cell culture and a drug-delivery carrier. Recently, its application as a scaffold for cells in tissue engineering has been reported by many researchers, who have concluded that silk fibroin represents a good material for use in regenerative medicine [9–17]. We also reported that chondrocytes cultured in fibroin sponge proliferated and synthesized cartilage-specific extracellular matrices (ECMs) and glycosaminoglycan [18]. It is particularly interesting that both proliferation and differentiation of chondrocytes occur simultaneously in our fibroin sponge, engendering good cartilage regeneration from a few seeded cells. Nevertheless, the mechanisms that play those roles in fibroin sponge material remain unknown.

Cell migration serves important roles not only in physiological and pathological events such as normal embryonic development, inflammation, wound healing, cancer metastasis and angiogenesis, but also in tissue reconstruction technology [19–23]. Cell migration is known to be affected directly or indirectly by various soluble growth factors [22, 24]. Cell migration is also known to depend strongly upon ECM structures and properties [21]. The chondrocyte behaviors in the fibroin sponge described above might be attributable to the properties of the fibroin surface to be prepared for use as an artificial ECM. Therefore, investigations of cell migration on the fibroin surface will yield important information to elucidate the advantages of fibroin material for tissue reconstruction. Nevertheless, no reported studies have examined cell migration on a fibroin surface.

In this study, cell migration on the silk fibroin surface was measured quantitatively for 24 h after contact with the surface. Those characteristics of migration were compared with characteristics observed on collagen and fibronectin surfaces as controls representing typical biomaterial surfaces. Time-dependent expression profiles of one ECM protein, transforming growth factor β-induced protein (TGFBI), at the early cell culture stage on the surfaces were assessed using qRT-PCR. For quantitative investigation of cell migration on surfaces, several techniques have been reported, including colloidal gold migration assay and single-cell tracking by time-lapse image capture with computer image analysis. We adopted the latter technique for direct quantitative measurements to support determination of the cell mobility on the fibroin surface. Results obtained in this study are expected to aid in the assessment of silk fibroin as a biomaterial used in tissue-engineering fields by revealing its effects on cell behavior.

2. Materials and Methods

2.1. Cell Culture

The murine fibroblast cell line NIH3T3 was grown in Eagle's medium (EMEM; Nissui) containing 10% FBS (Invitrogen), 2 mM L-glutamine (Invitrogen) and 0.1 mg/ml kanamycin (Invitrogen) in a humidified incubator (5% CO_2/95% air atmosphere at 37°C).

2.2. Preparation of Silk Fibroin Surfaces

Silk fibroin coating was performed on glass-bottomed dishes (35 mm diameter; Asahi Glass) or on cover glasses (15 mm diameter; Thermo Fisher Scientific) as follows. The silk fibroin aqueous solution was obtained by dissolving the degummed silk fiber of a *B. mori* silkworm cocoon with 9.0 M LiBr with subsequent dialysis against water. The fibroin aqueous solution was adjusted at 1% (w/v) concentration and was then deposited onto dishes and plates. After incubation for 30 min at room temperature, the fibroin solution was removed. Then the fibroin surfaces on the dishes and plates were dried in an oven at 50°C for more than 12 h. The fibroin surface was treated with 80% ethanol solution for 30 min at room temperature to render the fibroin surface insoluble by changing it from random to β-sheet conformation [25]. Finally the fibroin surfaces were dried at 50°C for more than 12 h. Before cell culture experiments, the fibroin surfaces were immersed in 70% ethanol solution for sterilization.

2.3. Preparation of Fibronectin and Collagen Surfaces

For use in this study, we prepared collagen and fibronectin surfaces as references for typical substrates used in cell culture and tissue engineering. The sterilized collagen solution (0.3 mg/ml) was prepared by dilution of Cellmatrix Type I-C (Nitta Gelatin) with 0.22-μm-filtered 1 mM HCl. A sterile fibronectin solution was prepared from fibronectin extracted from human plasma (Roche Diagnostics) for dissolution at the concentration of 50 μg/ml using autoclaved PBS (Dulbecco's Phosphate Buffered Saline; Wako). Each protein solution was applied to glass-bottomed dishes or cover glasses. Then each was kept for 30 min at room temperature and removed. Dishes and glasses were washed three times with autoclaved PBS. They were then used within 2 h for cell culture experiments. All procedures were conducted in sterile conditions.

2.4. Cell Migration

NIH3T3 cells were seeded on protein-treated glass bottom dishes and non-treated glass-bottomed dishes at a density of 2.5×10^4 cells/ml. After 1 h incubation, the medium was discarded and dishes were washed with medium to remove non-adherent cells. Then fresh medium was added to the dishes for the subsequent time-lapse experiment. Time-lapse microscopy was conducted at 5 min intervals for 24 h using a microscope (Olympus IX 70) equipped with a temperature-controlled

and CO_2-controlled chamber (MI-IBC, Olympus), a high-sensitivity cool CCD color camera (VB-7010, Keyence) and a digital microscope camera controller (VB-7000, Keyence). The average track distance per predetermined duration, or mileage, of cells on each sample surface (fibroin, collagen, fibronectin and glass) was tracked using MtrackJ software in ImageJ software (National Institutes of Health). MtrackJ is a freely available ImageJ plug-in that was produced to facilitate manual tracking in the image sequences and the measurement of the track statistics (http://www.imagescience.org/meijering/software/mtrackj/). The targeted cell positions at each time were determined by manual tracking using the MtrackJ function. Cell position data were exported to spreadsheets for calculation. The cell mileages on respective sample dishes were averaged from three individual cells. Statistically significant differences were inferred using t-tests.

2.5. *Quantitative Real-Time RT-PCR*

NIH3T3 were seeded on protein-treated glass-bottomed dishes and non-treated glass-bottomed dishes at density of 2.5×10^4 cells/ml. They were then cultured for 6, 24 and 48 h. After incubation, the cells were washed with PBS, removed with 0.25% trypsin-EDTA (Invitrogen) and centrifuged. Total RNA extraction from obtained NIH3T3 pellets and reverse transcription reactions were performed using a TaqMan Gene Expression Cells-to-CT Kit following the manufacturer's protocol. Custom probe-based TaqMan gene expression was used for quantitative RT-PCR reactions. Quantitative real-time PCR was performed using TaqMan custom probes with a StepOne Real-Time PCR System (Applied Biosystems). Relative expression levels were calculated as $2^{-\mathrm{ddCt}}$ after normalizing to the housekeeping gene, β-actin. Transforming growth factor, β-induced protein (TGFBI, NM_000358) was selected as a target gene.

2.6. *Cell Proliferation*

NIH3T3 cells were seeded on the fibroin-coated, the collagen-coated, and the fibronectin-coated 15-mm-diameter cover glasses or non-coated cover glasses at the density of 1×10^4 cells/glass. After 1, 3, 5 and 7 days incubation at 37°C/5% CO_2, the wells were washed with PBS to remove non-adherent cells. Then 0.5% Triton X-100 in PBS solution was added to each well to dissolve cells. Lactate dehydrogenase (LDH) activity of the cell-dissolving solutions was measured according to a description in a previous report [26]. The cell number at each time was determined according to the standard curve of the cell number against LDH activity. Then the data were averaged ($n = 5$). The doubling times of cells on the surfaces were calculated using exponential fitting.

3. Results

3.1. Cell Morphology

Figure 1 presents cell morphologies at 1 and at 25 h after incubation on fibroin (Fig. 1a and b), collagen (Fig. 1c and d), fibronectin (Fig. 1e and f) and glass (Fig. 1g and h) surfaces examined in this study from images captured during a time-lapse microscopy experiment. Figure 1 shows that the numbers of attached cells were similar on all surfaces. Some morphological differences among the four surfaces were observed (Fig. 1a, c, e and g). Almost all cells on the fibroin, collagen and glass adhered to the surface while maintaining their round shape with pseudopodia.

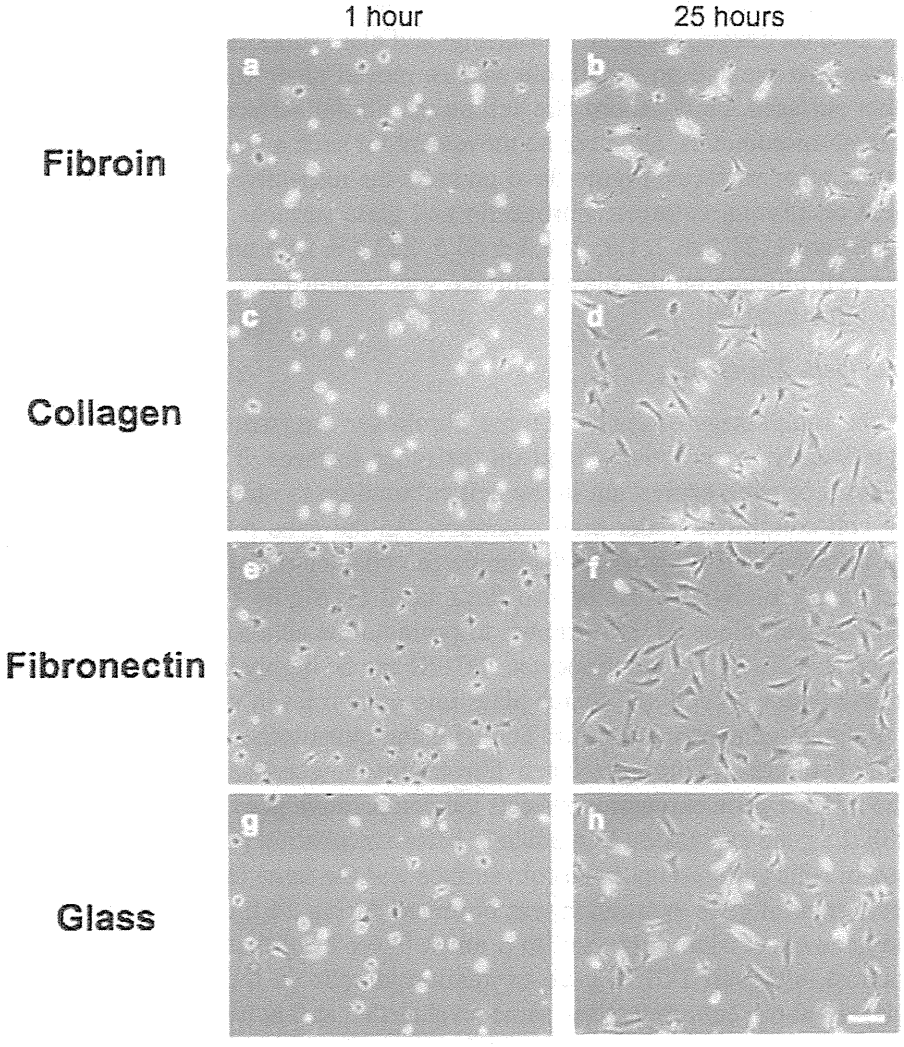

Figure 1. Cell morphology of NIH3T3 on (a, b) fibroin, (c, d) collagen, (e, f) fibronectin and (g, h) glass surfaces after (a, c, e, g) 1 and (b, d, f, h) 25 h seeding. Scale bar = 100 μm.

The other cells expanded on the surfaces. Almost all cells cultured on the fibronectin surface had begun to elongate at 1 h. Very few cells attached with a round shape (Fig. 1e). After 25 h incubation, the morphology of the cells cultured on collagen and glass expanded from a round shape, which resembled the morphology of the cells on fibronectin. It is particularly interesting that, on the fibroin surface, cells displayed similar morphology to that at 1 h incubation.

3.2. Cell Migration

To evaluate cell migration quantitatively on respective surfaces, we selected a target cell randomly in time-lapse images to trace its path using add-on MtrackJ software with ImageJ. Figure 2a–d portrays the average cell mileage for each 5 min during 24 h on fibroin, collagen, fibronectin and glass surfaces, respectively. Figure 2a shows that the cell on the fibroin surface moved much more actively than on the other surfaces. Furthermore, the cell on the fibroin surface traveled frequently for several micrometers, although no movement for such a long distance was observed on the other surfaces. Figure 3a–d presents the respective mileage data for movement on fibroin, collagen, fibronectin and glass surfaces. The respective average values are 1121.2 ± 211.9, 351.0 ± 64.5, 253.5 ± 24.5 and 293.7 ± 89.0 ($n = 5$). The cell mileage on the fibroin surface was significantly greater than mileage on any other surface.

3.3. Gene Expression

At the initial stage of contact on the fibroin surface (within 24 h), cells migrated significantly more actively than on the other surfaces. Therefore, we performed analysis of gene expression in the cell cultured on the fibroin surface to elucidate the cell conditions under high migration. As the gene related with cell mobility, we selected TGFBI gene to determine the characteristics of cells on the fibroin surface. Actually, TGFBI is also designated as βig-h3 (TGF-β-induced protein gene-human, clone 3). It is known to promote the adhesion and the spread of fibroblasts [27, 28]. In keratinocytes, TGFBI can be highly induced by transforming growth factor β (TGF-β), which plays important roles in wound healing [29–31].

Relative gene expression for TGFBI using quantitative RT-PCR after 6, 24 and 48 h of culture on fibroin, collagen, fibronectin and glass surfaces is shown in Fig. 4. The relative gene expression reflects the comparative gene expression at each time with the gene expression immediately before incubation (0 h). The TGFBI expression in cells cultured on the fibroin surface was the same level as 0 h culture at 6 h, but increased gene expression was observed during 24 h culture. At 48 h culture, the gene expression decreased to a much lower level than that before culture. In contrast, although TGFBI gene expression in cells on the glass and the collagen surfaces at 6 h culture was the same level as that at 0 h, as observed on the fibroin surface, the gene expression decreased at 24 h culture and became the same level as that on the fibroin surface at 48 h. Cells on the fibronectin surface displayed different TGFBI gene expression from the cells on other surfaces. At 6 h culture, a much

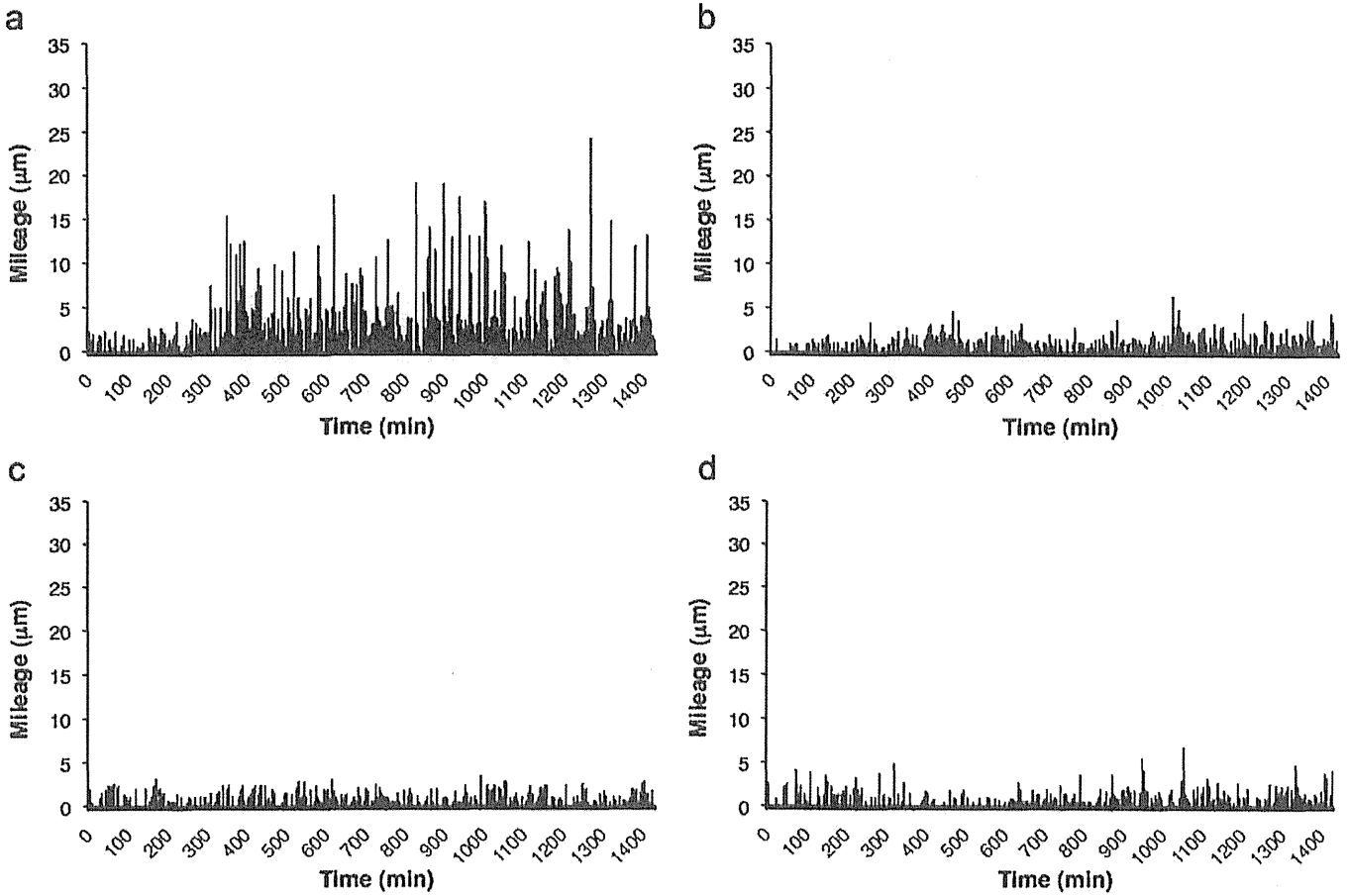

Figure 2. Migration of NIH3T3 on (a) fibroin, (b) collagen, (c) fibronectin and (d) glass surfaces was measured using time-lapse microscopy at 5 min intervals for 24 h.

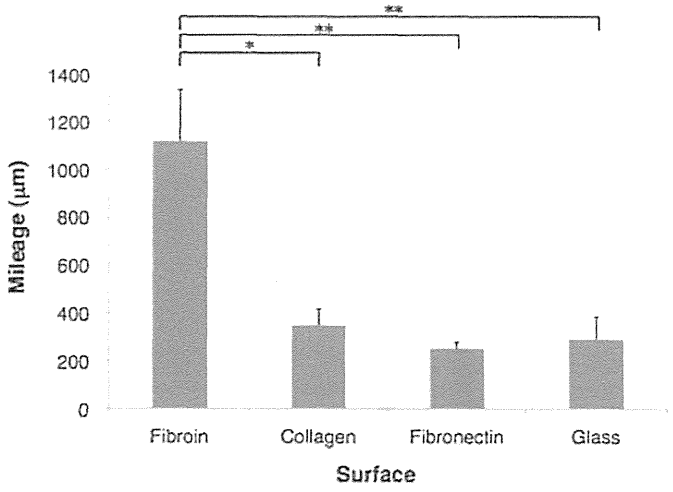

Figure 3. Average cell mileages of NIH3T3 on fibroin, collagen, fibronectin and glass surfaces ($n = 5$ cells). Pathways of NIH3T3 were tracked manually using the MtrackJ plug-in of ImageJ software for quantitative evaluation. $^{*}P < 0.0001$, $^{**}P < 0.00005$, significant differences between the indicated columns (by t-test).

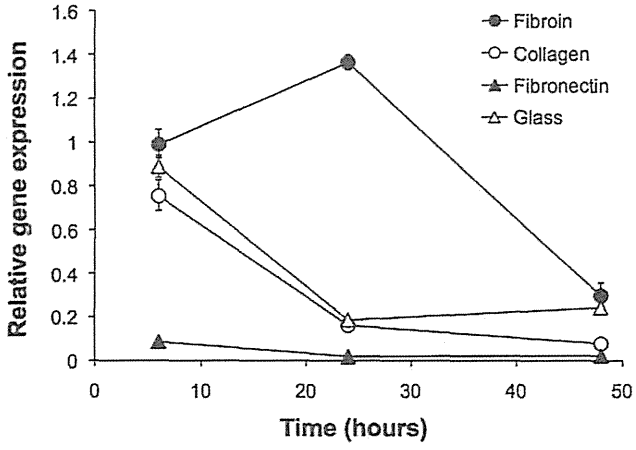

Figure 4. Relative mRNA expression levels of TGFBI in NIH3T3 on fibroin (●), collagen (○), fibronectin (▲) and (△) glass surfaces after 6, 24 and 48 h seeding. Quantitative RT-PCR was performed on total RNA extracted from NIH3T3. All dCt values were corrected for the efficiency of each primer set in relation to the housekeeping gene, β-actin.

lower level of gene expression in cells on the fibronectin surface was observed. The low gene expression persisted through culture until 48 h.

3.4. Cell Proliferation

The cell morphology and migration profile on the fibroin surface differed from those observed on the other surfaces within 24 h after contacting the surface, as described

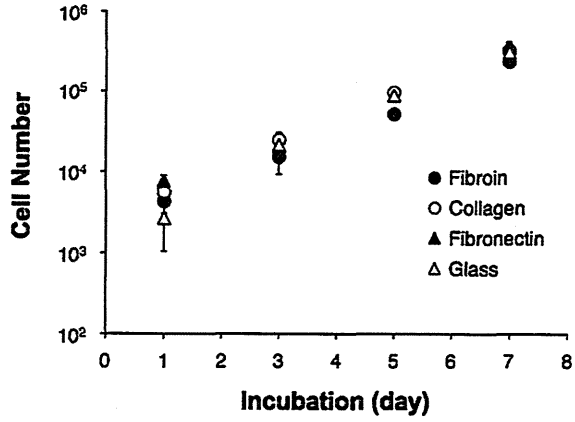

Figure 5. Cell growth curves on fibroin (●), collagen (○), fibronectin (▲) and (△) glass surfaces. Cell numbers on the five surfaces on each culture day were averaged.

Table 1.
The doubling times of NIH3T3 cells cultured on various surfaces

	Surface			
	Fibroin	Collagen	Fibronectin	Glass
Doubling time (h)	23.9 ± 3.2	25.5 ± 1.7	23.6 ± 1.1	24.6 ± 2.6

above. To ascertain cell behavior on the fibroin surface at longer contact times, more than 24 h, we examined cell proliferation on the fibroin surfaces in comparison with that on other surfaces. Cell proliferation is a basic cell function that is reflected in surface properties such as physicochemical, biological and toxicity properties. Figure 5 presents the cell growth curves for growth on fibroin, the collagen, the fibronectin, and the glass surface. Cell doubling times are shown in Table 1. Cells can proliferate normally on the fibroin surface just as they can on the other surfaces. This result indicates that cells on the fibroin surface perform just as they do on other surfaces after 24 h contact with the surface.

4. Discussion

Cell mobility on biomaterials influences the biomaterials' biocompatibility through inflammatory reactions, wound healing and tissue reconstruction [19–22, 32, 33]. We conducted quantitative assay of the NIH3T3 cell migration on the fibroin surface by tracking a single cell from time-lapse images, and compared those images with some obtained for collagen and fibronectin surfaces, which are ECM components, as control surfaces for typical biomaterials. Results show that cells move much more actively on the silk fibroin surface than on the collagen and fibronectin surfaces. Few reports in the literature describe the quantitative determination of

cell mobility by direct measurement of a single cell. Harris *et al.* reported results of a quantitative assay of cell migration on laminin and fibronectin substrates using time-lapse experimentation [32]. They reported the respective cell migration speeds on fibronectin surface as 0.44 ± 0.21 and 0.91 ± 0.37 μm/min for human epidermal sarcoma A431 and human fibrosarcoma HT-1080. Figure 3 shows that the average migration speed of the NIH3T3 cells on the fibronectin surface during 24 h was estimated as 0.18 ± 0.02 μm/min. The migration speed is apparently much lower than that reported by Harris *et al.* [32]. However, Fig. 2 shows that the speed of NIH3T3 cell migration on the fibronectin surface during each 5 min was estimated as 0–0.13 μm/min. Therefore, our results will be useful for comparison with reported results, even though a different cell line was used.

Li *et al.*, using the colloidal gold migration assay, compared human dermal fibroblast motility on collagen I, collagen IV, fibronectin, vitronectin and poly(L-lysine) surfaces with or without platelet-derived growth factor-BB (PDGF-BB) [21]. The fibroblast on the collagen I surface showed the highest migration among all surfaces. The fibroblast migration on the collagen surface was reportedly about twice as high as that on the fibronectin surface. In our experiment, the average migration speed of NIH3T3 cell on the collagen surface was 0.24 ± 0.04 μm/min, which is similar to that on the fibronectin surface. Results of this study agree with the reported results, indicating that a silk fibroin surface can support higher cell mobility than either the collagen or the fibronectin can. The cell morphology is correlated with cell mobility: round cells moved actively on the surface, but the mobility of the spread-shaped cells was low. Especially on the fibronectin surface, almost all cells were spread from initial contact at 1 h culture. The lowest cell mobility was observed in the fibronectin surface. At 25 h culture, most cells on the collagen, fibronectin and glass surfaces showed spreading morphology, although round cells remained on the fibroin surface, where the highest cell mobility was observed. The expression of TGFBI was also correlated with the cell morphology. At both 1 and 25 h culture, most cells showed a spreading morphology and low expression of TGFBI on the fibronectin surface. In contrast, the round cells on the fibroin surface retained high expression of TGFBI after 6 and 24 h culture.

The expression of the TGFBI gene in the cells cultured on the fibroin surface had increased during 24 h culture, although the expression on the other surfaces was lower than that before culture. TGFBI is an ECM protein that is highly induced by TGF-β [27, 28]. Therefore, it is probable that TGF-β was produced by cells on the fibroin surface during the 24 h culture. TGF-β is known to be able to stimulate ECM synthesis, as can the collagen and fibronectin, and to increase fibroblast and neutrophil mobility with subsequent acceleration of wound healing and tissue construction [29–31]. Several groups have reported that cell adhesion to the TGFBI coated surface was dramatically greater than that to the BSA-coated surface [28, 34], which suggests that the NIH3T3 cells cultured on the fibroin surface are active to accelerate the production of ECM proteins through the TGF-β and TGFBI secretion during early culture. In contrast, the ECM protein production is not accelerated